ACS APPLIED MATERIALS & INTERFACES

Research Article

www.acsami.org

# Self-Powered UV-vis Photodetector Based on $ZnIn_2S_4$/Hydrogel Interface

Lily Mandal, Nilima S. Chaudhari, and Satishchandra Ogale*

Centre of Excellence in Solar Energy, Physical and Materials Chemistry Division, National Chemical Laboratory (CSIR-NCL), Pune, Maharashtra 411008, India

Supporting Information

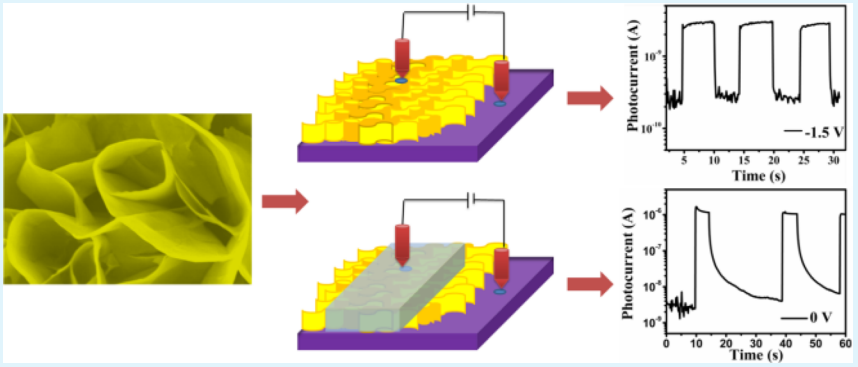


**ABSTRACT:** The photosensing properties of vertically aligned $ZnIn_2S_4$ nanopetal films grown hydrothermally on FTO coated glass are examined without and with surface dispensed agarose gel. For the $ZnIn_2S_4$ nanopetals photodetector (without gel) there is no photoresponse for zero bias. Most interestingly, with surface dispensation of agarose gel, the hybrid electronic-iontronic interface system shows a strong photoresponse even under zero bias, a highly efficient self-powered UV-visible light photodetector. Indeed, the zero bias $ZnIn_2S_4$/gel hybrid photoresponse is a factor of 100 stronger as compared to the response of the only $ZnIn_2S_4$ device (at −1.5 V bias) and that too without any significant degradation in response time. The possible operating mechanisms are proposed.

**KEYWORDS:** *$ZnIn_2S_4$, agarose gel, photodetector, UV-vis, hybrid device, impedance spectroscopy*

## INTRODUCTION

Metal chalchogenides have attracted considerable attention from the optoelectronics community lately due to their interesting semiconducting and optical properties. Indeed there is a significant current interest in sulfide based photodetectors.[1−3] Zinc indium sulfide ($ZnIn_2S_4$) is one such ternary chalcogenide with layered structure and has applications in the fields of charge storage, photocatalysis, and photovoltaics.[4−7] The optical absorption of $ZnIn_2S_4$ corresponds well to the solar spectrum, rendering it a material of growing interest in the context of solar optoelectronics. Various nanostructures of $ZnIn_2S_4$ such as nanotubes, nanorods, and microspheres have been fabricated to tune the physical and chemical properties to the desired specifications.[4−9] To the best of our knowledge however no $ZnIn_2S_4$-based photodetector is reported thus far.

There are two polymorphs of $ZnIn_2S_4$ namely cubic and hexagonal,[8,9] and it would be interesting to explore both of them. However since the morphologies need to be similar for proper comparison, this will form a part of our ongoing efforts. Hence here we focus on the hexagonal form which we could synthesize in the desired 2D morphological form. The 2D nanostructures are especially important because of high surface area and efficient charge transport. In many cases substrate-supported 2D $ZnIn_2S_4$ nanostructures can be easily grown, but their incorporation into robust device systems is not trivial due to issues related to the nature and degree of surface coverage of subsequent layers that can be realized for the creation of functional heterostructure configurations. An interesting approach to make a shape-conforming contact to an orientationally disordered nanostructure is by using a functional liquid or gel, which is transparent and conducting. Ionic liquids or gels represent good candidates in this respect.

Another objective was to explore the possibility of a realizing self-powered photodetector in view of the charge separation (photovoltaic effect) character of the interfaces formed. Indeed, recently there is a surge of interest in self-powered nanodevices, especially photodetectors. Several structures are possible to observe photovoltaic effect: p-n junctions, heterojunctions, Schottky barriers and metal insulator-semiconductor (MIS) photocapacitors. Various self powered Schottky,[10] p-n junction,[11,12] or photoelectrochemical cell (PECC) type[13,14] photodetectors have thus been reported.

Received: June 28, 2013
Accepted: August 26, 2013
Published: August 26, 2013

   dx.doi.org/10.1021/am4025356 | ACS Appl. Mater. Interfaces 2013, 5, 9141−9147

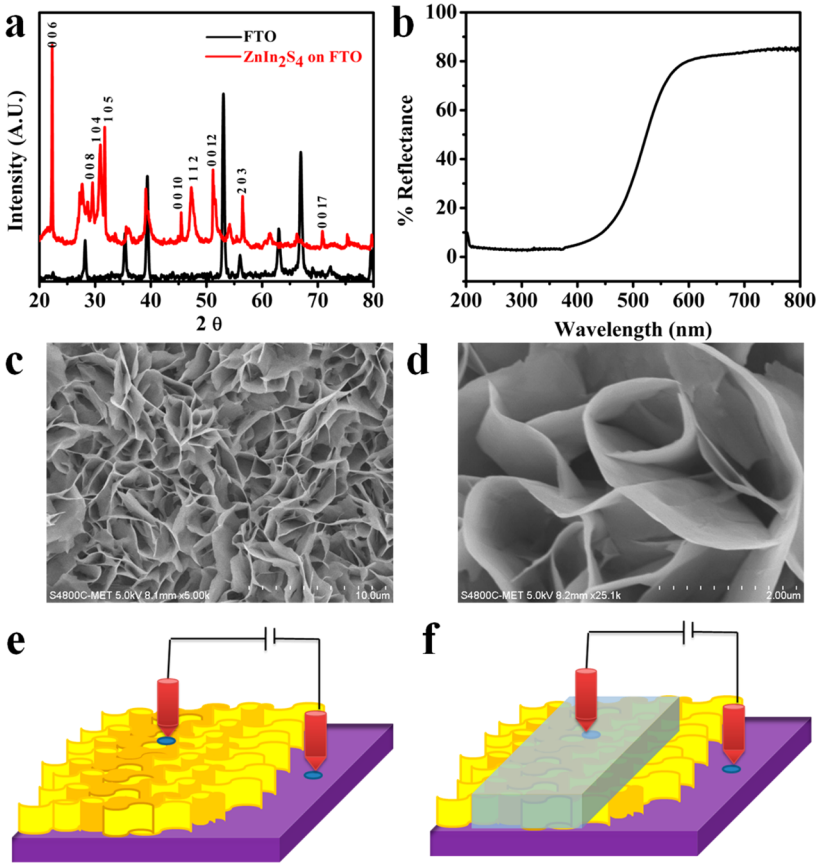


**Figure 1.** (**a**) XRD, (**b**) DRS, (**c**),(**d**) FE-SEM of $ZnIn_2S_4$ vertically aligned sheets on FTO coated glass, (**e**) device architecture of FTO-$ZnIn_2S_4$-Pt, and (**f**) FTO-$ZnIn_2S_4$-agarose gel-Pt device.

Recently, there is a growing interest towards developing ion-based devices such as rectifiers, logic gates, memresistors, transistors, etc. which mimic the biological system in their mode of operation; notably the signal transport in neurons occurs via ionic transport.[15−19] Agarose-based hydrogel has attracted a lot of interest towards developing such iontronic devices, since it has good ionic conductivity ($H^+$ and $OH^-$ ions). We recently demonstrated an electronic/ionic hybrid photodetector comprised of ZnO nanorods and agarose gel, which showed a remarkable three orders of magnitude strong and fast UV photoresponse as compared to that of only ZnO nanorods.[20] In this work our intent was to apply the concept of gel induced manipulation of interface phenomena to $ZnIn_2S_4$ based photosensing to realize a strong and fast response over the UV-visible regime.

In this work vertically-aligned dense $ZnIn_2S_4$ nanopetal films were grown on FTO glass by a hydrothermal method and evaluated for their photoresponse in different interesting device configurations. The petals in the film are well-separated from each other, and the separation between two successive petals is in the range of 200−1000 nm. This indicates that the film surface is highly accessible for an interface-based device configuration. Large surface to volume ratio and low dimensionality are known to yield higher light sensitivity and increase the photocarrier lifetime as more charge separation take place due to surface states.

Here, we demonstrate that the UV-vis photoresponse of vertically aligned $ZnIn_2S_4$ film is enhanced by three orders of magnitude by modifying its surface with a hydrogel. The performance of such a hybrid device is compared to that of a $ZnIn_2S_4$ based photodetector without gel. Such a huge enhancement in photoresponse and zero bias (self-powered) operation is attributed to unique features of the interface between the gel and the nanostructured $ZnIn_2S_4$ film.

## EXPERIMENTAL SECTION

To obtain a uniform film of $ZnIn_2S_4$ on the FTO substrate, first we cleaned the FTO and dried at 450 °C for 2 h. Zinc acetate, indium nitrate, and thiourea were used as precursors of Zn, In, and S, respectively. 1 mmol of zinc acetate, 2 mmol indium nitrate, and double excess (8 mmol) thiourea were dissolved in deionized water. This mixture was stirred for 30 min and transferred to a Teflon-lined reactor. Cleaned FTO-coated glass substrates were hung in the reactor with the help of Teflon tape. The autoclave was then sealed and maintained at 150° C for 16 h, followed by natural cooling to room temperature. A yellow film was seen to grow on the FTO substrate which was further washed with DI water and finally with ethanol. This film was dried under IR for further characterizations.

All the samples were characterized by X-ray diffraction (Philips X'pert Pro), scanning electron microscopy (SEM), diffuse reflectance spectroscopy (DRS) recorded with an integrated sphere, electrochemical impedance spectroscopy (EIS, Auto lab PGSTAT 30), and quantum efficiency using Newport IPCE measurement setup. The current voltage (I−V) measurements were done using Keithley 2400 SMU. Photoconductance was measured using LEDs of different wavelengths and solar simulator model Newport AM 1.5 1 Sun. All the electrical measurements were done inside a dark room under ambient conditions.

## RESULTS AND DISCUSSION

Figure 1a depicts the comparison between the X-ray diffraction patterns of FTO coated glass and $ZnIn_2S_4$ (ZIS) on FTO coated glass. It is clearly seen from Figure 1a that hexagonal $ZnIn_2S_4$ is


dx.doi.org/10.1021/am4025356 | ACS Appl. Mater. Interfaces 2013, 5, 9141−9147

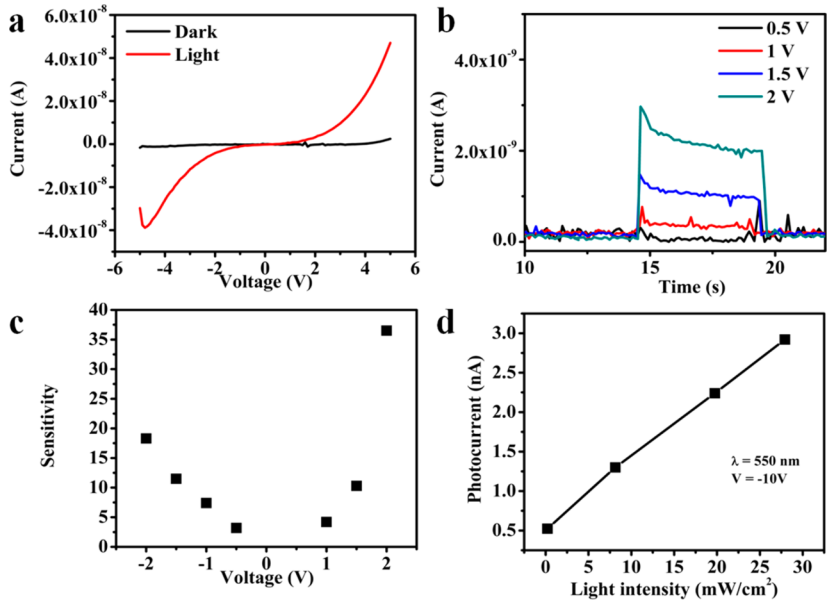


**Figure 2.** (**a**) I–V under dark and illumination, (**b**) photoresponse as a function of time with light chopping in a semilog plot at different bias voltage, (**c**) sensitivity as a function of applied bias for FTO-$ZnIn_2S_4$-Pt device, (**d**) photocurrent as a function of illumination intensity.

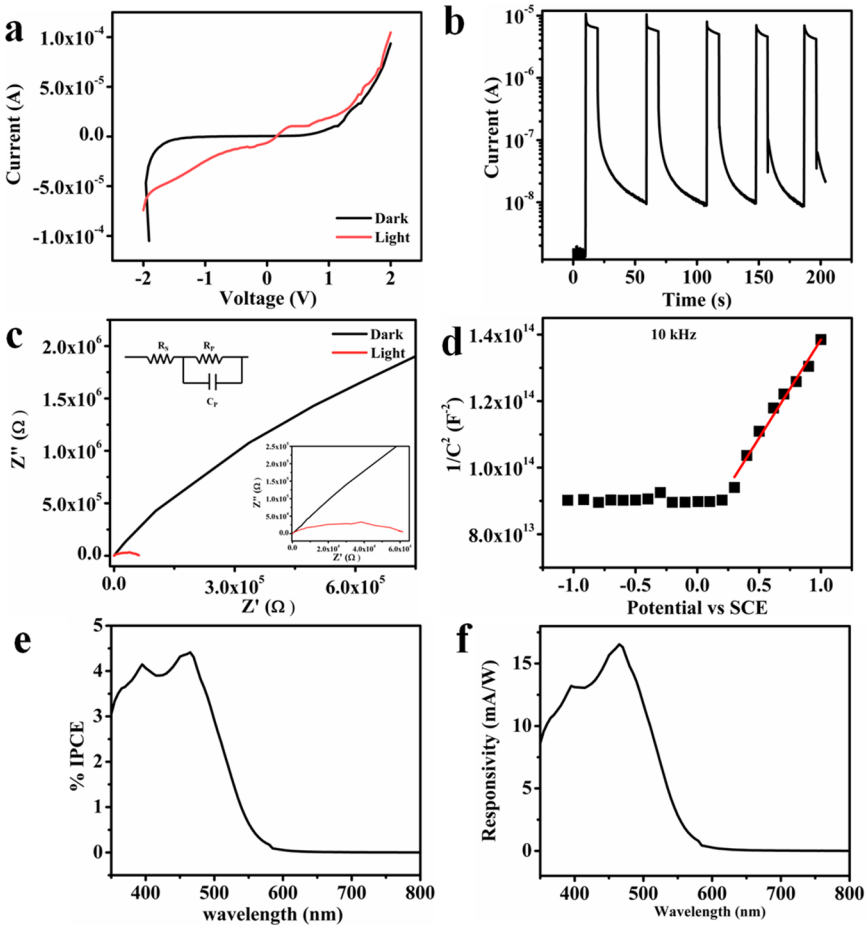


**Figure 3.** (**a**) I–V under dark and illumination, (**b**) photoresponse as a function of time with light chopping in a semilog plot at 0 bias, (**c**) impedance plot inset shows magnified response at high frequency and fitted equivalent circuit, (**d**) Mott-Schottky plot of $ZnIn_2S_4$ agarose gel, (**e**) IPCE of FTO-$ZnIn_2S_4$-agarose gel-Pt under dark and illumination, (**f**) responsivity as a function of wavelength $ZnIn_2S_4$ agarose gel.

successfully grown on the top of conducting FTO glass. This result is in good agreement with the reported JCPDS data (ICDD-JCPDS card No. 72-0773). The UV-visible diffuse reflectance spectrum (UV-vis-DRS) is shown in Figure 1b. It shows a fairly sharp absorption edge indicating homogeneous and stoichiometric ZIS film formation. Strong absorption in the


dx.doi.org/10.1021/am4025356 | ACS Appl. Mater. Interfaces 2013, 5, 9141–9147

visible region at 515 nm implies that this material is favorable for visible light photocatalysis and photodetectors applications. The morphology of the ZIS film deposited on the FTO substrate observed by FE-SEM is shown in Figure 1c,d. Uniform growth of vertically aligned petals with large density is clearly seen. The mean thickness of the petal is noted to be ~20 nm. These petals are well spaced from each other, and the separation between two successive petals is in the range of 200−1000 nm. This indicates that the film is highly open-structured, and this characteristic is useful to access its full surface area.

Figure 1e and 1f show the schematic of the FTO-$ZnIn_2S_4$-Pt electronic device and the FTO-$ZnIn_2S_4$-agarose gel-Pt electronic-ionic hybrid device, respectively. In both of these devices FTO-coated glass serves as the bottom electrode and the Pt tip acts as the top electrode. In the hybrid device the $ZnIn_2S_4$ nanopetal film was covered with a layer of agarose solution and cooled to room temperature for gellation. For all I−V measurements the FTO contact was grounded and potential was applied through the Pt tip. The I−V curves for the FTO-$ZnIn_2S_4$-Pt device under dark and solar AM 1.5 1 Sun illumination are shown in Figure 2a. The nonlinearity of the I−V curves in the dark indicates that the contact between the $ZnIn_2S_4$ film and Pt/FTO electrode is a Schottky contact. For the above device the dark current is in the range of $10^{-10}$ A. Such a low dark current is a requisite to achieve a high sensitivity of a given photodetector.

Figure 2b shows the dynamic photoresponse of the FTO-$ZnIn_2S_4$-Pt system under solar illumination with a power density of 100 mW/cm$^2$ at different bias voltages. The dynamic photoresponse was measured by chopping the light source for 5 s manually and measuring the current as a function of time using Keithlay 2400 SMU. The generated photocurrent increases with increasing bias voltage indicating that a greater number of photogenerated carriers gets converted to photocurrent with higher bias voltage. The photocurrent increases due to the reduction of the carrier transit time resulting in efficient separation of charge carrier or reduced recombination by the applied bias. When the illumination is on, the current in the FTO-$ZnIn_2S_4$-Pt system increases rapidly, whereas when the illumination is off the current first decreases rapidly and then slowly reaches saturation. The rise time is defined as the time taken by the photodetector to reach 90% of maximum photocurrent from its dark current value, and the reset (recovery) time is the time taken to reach 1/e times the maximum photoresponse current. To measure the response time of the photodetector more precisely it was connected in series to a 1 MΩ resistor and oscilloscope. The photodetector was placed below the light source with chopper. Then the photovoltage drop across the resistor was measured as a function of time. The $ZnIn_2S_4$ device shows the rise time and reset times of only 2 ms (see Supporting Information SI−I). Such fast photoresponse can be attributed to efficient generation/separation and recombination of the photocarriers. The sensitivity of the device defined as the ratio of photocurrent to dark current is also plotted as a function of bias voltage and shown in Figure 2c. The corresponding value increases with an increase in the bias voltage. Figure 2d shows the photocurrent as a function of light intensity. A green LED of wavelength 550 ± 20 nm was used as the light source; the photocurrent is seen to increase linearly with increasing light intensity.

Figure 3a shows the current voltage (I−V) characteristics of the ZIS-agarose gel hybrid device in the dark and under solar simulator AM 1.5 1Sun (100 mW/cm$^2$) illumination. The addition of agarose gel modifies the interface (see Supporting Information SI−II and SIII) in such a manner that the FTO-$ZnIn_2S_4$-agarose gel-Pt hybrid system is more rectifying as compared to the FTO-$ZnIn_2S_4$-Pt device. The $ZnIn_2S_4$/gel case shows a rectification ratio of 48 at ±1 V, and there is an increase in the dark current as compared to the $ZnIn_2S_4$ device without gel. The striking feature of the $ZnIn_2S_4$/gel system is the photovoltaic effect i.e. the system has an open circuit voltage of 0.63 V with a current density of 7 $\mu$A/cm$^2$ under solar illumination. This open circuit voltage is due to the specific nature of the $ZnIn_2S_4$/gel interface. This voltage allows rapid and efficient separation of charge carrier and prohibits recombination even at zero applied bias. Thus, the FTO-$ZnIn_2S_4$-agarose gel-Pt hybrid device is a self-powered hybrid photodetector.

In the hybrid device it can be seen that in sweeping the bias voltage from −2 V to +2 V in the dark the current minimum occurs at around −1 V, whereas under illumination it shifts toward positive bias (shown in a semilog I−V plot in Supporting Information SI−III). This can be attributed to the characteristic electronic-ionic nature of the interface. In the $ZnIn_2S_4$ film in contact with an electrolyte, a space charge region develops within $ZnIn_2S_4$, Helmholtz EDL develops at the interface with the gel, and a diffuse charge layer (Stern layer) develops in the gel due to electron-ion imbalance.[21] The interface is a combination of space charge capacitance, Helmhotz capacitance, and the Stern capacitance. When this interface is illuminated, high density of electrons and holes is generated which changes the interface charge distribution, thereby dramatically reducing the capacitances of the interface regions and shifting the current minimum significantly towards positive bias. This is further confirmed by impedance spectroscopy.

Figure 3b shows the dynamic performance of the $ZnIn_2S_4$/gel hybrid device under AM 1.5 1 Sun illumination for zero bias condition. The device shows a remarkably strong photoresponse ($I_{light}/I_{dark}$) of 3 orders of magnitude (a factor of 1000) and thus works as a highly efficient self-powered photodetector. In the FTO-$ZnIn_2S_4$-Pt device without gel the highest photocurrent value was only in the region of $10^{-9}$ A, which is very low and does not meet the requirements of practical application.

When the light is on, the current increases rapidly reaching a maximum and then decreasing gradually to reach a stable value. The decrease in current after reaching the maximum is due to the recombination of the photogenerated charge carriers. In the hybrid ($ZnIn_2S_4$/gel) device there is diffusion and drift of charge carriers on the gel and $ZnIn_2S_4$ sides, respectively, and with diffusion being a slow process the accumulation of charge carriers can occur near the interface causing a higher rate of recombination under constant illumination, especially under zero bias. When the light is off, the current initially decreases rapidly and then gradually reaches saturation. The rise time for a hybrid device is about 25 ms. Decay response time constant of the device is 120 ms (see Supporting Information SI−IV). The initial fast response is attributed to the photoexcited carrier generation, and the slow response at the second stage is mainly ascribed to photodesorption of the chemisorbed oxygen ions and water molecules from the surface of the $ZnIn_2S_4$. The response time of the hybrid device is understandably slower as compared to the $ZnIn_2S_4$ device without gel. The $ZnIn_2S_4$ device without gel is a pure electronic device as against the $ZnIn_2S_4$-gel device which is a hybrid device working at zero bias. In the hybrid device the transport of charges through the gel occurs by diffusion, which is a slower process than pure electronic transport, hence the response is somewhat slower.

To gain a better understanding of the electronic−ionic interface of the hybrid devices the electrochemical impedance spectroscopy (EIS) was performed in the dark and under AM1.5 1 Sun illumination in the frequency range of 10 mHz to $10^6$ Hz at an ac voltage of 10 mV. The impedance was recorded in a two-electrode setup. Figure 3c shows the Nyquist plot for the $ZnIn_2S_4$ gel system. The enhanced performance of the hybrid device can be noted from the difference in the impedance spectra in the dark and under illumination. In the dark, the impedance plot shows a roughly straight (slightly bowing) line over the entire frequency regime. Under illumination the impedance plot shows one semicircle. The obtained data was fitted into an equivalent circuit, and the fitted values are given in Table 1. $R_S$ represents the contact resistance between FTO/$ZnIn_2S_4$ and gel/Pt, and it remains nearly constant under dark and illumination. $R_{P1}$ represents the charge transfer resistance, and its value is drastically reduced from 2.54 MΩ in the dark to 61.3 kΩ under illumination.

**Table 1. Fitted Impedance Parameter**[a]

| | $R_S$ [Ω] | $R_P$ [kΩ] | $C_P$ [μF] |
|---|---|---|---|
| dark | 27.9 | 2540 | 4 |
| light | 27.2 | 61.3 | 4.7 |

[a] $R_S$ represents the contact resistance, and $R_{P1}$ represents the charge transfer resistance.

To calculate the carrier density, flat band potential, carrier type, and carrier density the Mott-Schottky plot was recorded for the $ZnIn_2S_4$/gel based hybrid system.[20] In the Mott Schottky plot $1/C^2$ is plotted against the applied potential. The intercept of the linear portion of $1/C^2$ on the $x$-axis gives the value of the flat band potential, and the slope of the curve gives the charge carrier density. Figure 3d shows the Mott-Schottky plot for the case of $ZnIn_2S_4$/gel. The positive slope of the Mott Schottky plot shows that the as-grown $ZnIn_2S_4$ is n-type. The charge density can be calculated by,

$$N_d = \left(\frac{2}{e_0 \varepsilon \varepsilon_0}\right)\left[\frac{d\left(\frac{1}{C^2}\right)}{dV}\right]^{-1}$$

where $\varepsilon_0$ is permittivity of free space, $\varepsilon$ is the dielectric constant of $ZnIn_2S_4$, $e_0$ is electronic charge, $N_d$ is carrier density, and $V_{FB}$ is the flat band potential. The calculated carrier density of $ZnIn_2S_4$ in the presence of agarose gel is $5.5 \times 10^{16}$ $cm^{-3}$. The flat band potential calculated from the intercept is −0.16 V.

The incident photon to current conversion efficiency (IPCE) for the $ZnIn_2S_4$/gel system in the spectral range of 350−800 nm is shown in Figure 3e. To measure the IPCE a $ZnIn_2S_4$ film of area 0.25 $cm^2$ was first protected on all the sides by Scotch tape, and then the film was covered with a thin layer of agarose gel. Transparent platinized FTO was used as a counter electrode. The IPCE shows that the hybrid $ZnIn_2S_4$/gel system absorbs mostly in UV and visible up to 600 nm. The IPCE corresponds well with the DRS spectrum for the $ZnIn_2S_4$ film. The IPCE however shows two maxima corresponding to 3.13 eV and 2.61 eV which can be attributed to the complex band structure due to changes in the concentration and types of structural defect in these $ZnIn_2S_4$ films.[22] The IPCE gives the EQE as a function of wavelength for zero bias.[23]

Figure 3f shows the spectral responsivity of the $ZnIn_2S_4$-gel-Pt photodetector at zero bias. Spectral responsivity is a measure of the photocurrent flowing in the detector divided by incident optical power. The responsivity was calculated from EQE taking the photoconductive gain as 1.

$$R_\lambda = \frac{(EQE)}{h\nu}$$

As can be seen, the $ZnIn_2S_4$-gel-Pt hybrid photodetector has a responsivity of 16.5 mA/W at 470 nm even for zero bias. This is due to the efficient separation of charge carrier at the interface by the open circuit voltage. The spectral responsivity of the device is indeed good.

Figure 4a shows the band diagram for the FTO-$ZnIn_2S_4$-Pt system. The photoconduction in $ZnIn_2S_4$ occurs due to the generation of electron-hole pairs in the presence of light. The holes get trapped by the acceptor level existing above the valence band of $ZnIn_2S_4$. Trapping of holes creates charged acceptor levels. These charge acceptor levels repel the electron, thereby preventing the recombination. Thus an electron can move freely through the material leading to an increase in conductivity in the presence of light.[7]

The $ZnIn_2S_4$ agarose gel device basically acts as metal insulator-semiconductor (MIS) photocapacitor. The electronic/ionic nature of the interface of $ZnIn_2S_4$ and agarose gel is expected to be defined by the differences in the Fermi level of $ZnIn_2S_4$ and the redox potential of agarose gel.[24] This leads to band bending in $ZnIn_2S_4$ resulting from the transfer of carriers across the interface: in this case electron transfer from $ZnIn_2S_4$ to the agarose gel and hole transfer in the opposite direction. This would cause a depletion region in $ZnIn_2S_4$ and an electric double layer plus a Stern layer in the gel with accumulation of $OH^-$ at the $ZnIn_2S_4$ surface. Thus, at the interface an in-built potential develops as confirmed by $V_{oc}$ of 0.63 V. This built-in electric field causes the charge carriers of opposite sign to move in opposite directions depending upon the external circuit. When the interface is illuminated by light the electron-hole pairs are generated within the $ZnIn_2S_4$. The electron-hole pairs generated at the interface are efficiently separated by the built-in potential due to the depletion region at the interface. The electron gets

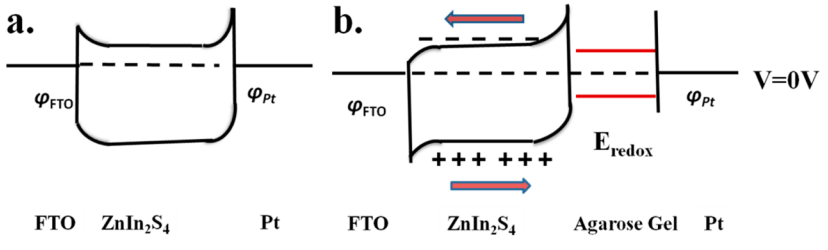


**Figure 4.** Band diagram: (**a**) $ZnIn_2S_4$ nanopetal device and (**b**) $ZnIn_2S_4$-agarose gel hybrid device at 0 V.


dx.doi.org/10.1021/am4025356 | ACS Appl. Mater. Interfaces 2013, 5, 9141−9147

**Table 2. Comparison of the Critical Parameters for the Photodetectors**

| photodetector | type | photosensitivity | rise/fall time | operating voltage (V) | responsivity(A/W) | reference |
|---|---|---|---|---|---|---|
| $MoS_2$ | phototransistors | - | 50 ms | - | $7.5 \times 10^{-3}$ | 2 |
| GaS nanosheet | photoconductor | $1.5 \times 10^4$ | 30 ms | 2 | 4.2 | 3 |
| GaSe nanosheets | photoconductor | 0.38 | 0.02 s | 2 | 2.8 | 4 |
| Sb-doped ZnO | Schottky | 2200 | 100 ms | 0 | - | 11 |
| ZnO/GaN | p-n | $10^6$ | 20/219 $\mu$s | 0 | - | 12 |
| ZnO nanorods/CuSCN | p-n | $10^5$ | 500 ns/6.7$\mu$s | 0.1 mV | $1 \times 10^{-3}$ | 13 |
| $TiO_2/SnO_2$ | PECC | 4550 | 0.03 s/0.01 s | 0 | 0.6 | 14 |
| $TiO_2$ | PECC | 2698 | 0.08s/0.01s | 0 | - | 15 |
| ZnO/agarose gel | hybrid | >1000 | 250/100 ms | 2 | $1.3 \times 10^{-2}$ | 7 |
| $ZnIn_2S_4$ without gel | Schottky | >10 | 2 ms/2 ms | 1.5 V | - | present work |
| $ZnIn_2S_4$/agarose gel | hybrid | >1000 | 25 ms/120 ms | 0 | $1.6 \times 10^{-2}$ | present work |

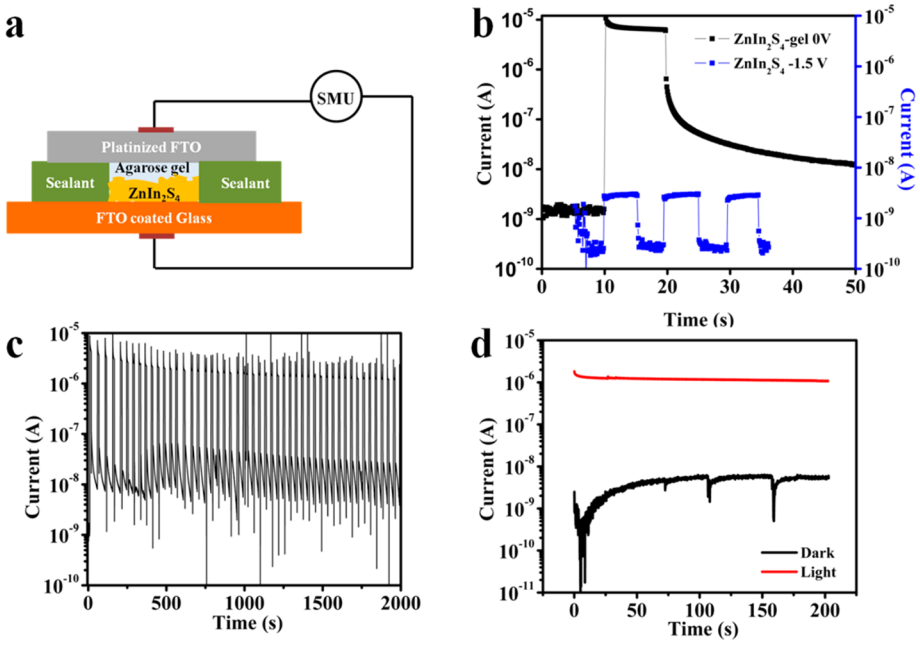


**Figure 5.** (**a**) Schematic of $ZnIn_2S_4$–gel sealed hybrid device, (**b**) comparison of photoresponse of $ZnIn_2S_4$ –gel hybrid device at 0 V with $ZnIn_2S_4$ device at −1.5 V, (**c**) and (**d**) show the stability of the sealed device.

transferred to the FTO from $ZnIn_2S_4$, and the holes move through the gel.

When the performance of only the $ZnIn_2S_4$ photodetector (i.e. without gel) is compared to other sulfide ($MoS_2$, GaS, GaSe) based detectors,[2−4] it shows a relatively faster response. The $ZnIn_2S_4$ device also shows better photosensitivity as compared to a GaSe photodetector at comparable operating voltage.[4] The $ZnIn_2S_4$-gel photodetector can now be compared to other photodetectors based on the use of p-n junction, Schottky junction, and PECC (photoelectochemical cell). This comparison is shown in Table 2. The hybrid device shows a comparable response time and sensitivity to Schottky and PECC type photodetectors at zero bias. However, the response time of the p-n photodiode is better than our hybrid photodetector.

We also evaluated the performance of a doctor-bladed thin film of $ZnIn_2S_4$ with that of the vertically aligned $ZnIn_2S_4$ nanopetal film, and the corresponding results are discussed in Supporting Information SI−V. This was done to understand the possible negative consequences of the petal-like morphology and related light shadowing effects. It was found that the performance of the doctor-bladed $ZnIn_2S_4$ thin film *without gel* is seen to be better than that of the vertically aligned nanopetals film *without gel*. Interestingly, however, in the case of gel-based devices the performance of the $ZnIn_2S_4$ nanopetal-gel photodetector is found to be better in comparison to the doctor-bladed $ZnIn_2S_4$ thin film-gel photodetector. This can be attributed to nanopetal morphology which enhances the interface area between the $ZnIn_2S_4$ and agarose gel. It should be noted that after the pouring of gel there is ample opportunity for internal refraction effects within the configuration which can access the so-called shadow regions in the absence of the gel.

Figure 5b shows the photoresponse comparison of the FTO-$ZnIn_2S_4$-gel-Pt hybrid device at zero bias and the FTO-$ZnIn_2S_4$-Pt device at −1.5 V bias. The response of the hybrid device even for zero bias is 100 times higher than that of the only $ZnIn_2S_4$ device. To make a robust and realistic device we covered the $ZnIn_2S_4$ nanopetals film of area $0.5 \times 0.5$ cm$^2$ on all the sides by a sealant; and then a platinized FTO with two drilled holes was applied as a top contact. The device was thus sealed. Finally, agarose gel was dispensed on the surface of the $ZnIn_2S_4$ nanopetals through the holes with the help of vacuum pump. These holes were also sealed using the same sealant. Figure 5a shows the schematic of this device and the corresponding photoresponse as a function of time during alternating light on/off in air at zero bias. The device shows a stable performance as


dx.doi.org/10.1021/am4025356 | ACS Appl. Mater. Interfaces 2013, 5, 9141−9147

confirmed by Figure 5c and d. Figure 5c shows the light chopping data for 50 cycles.

## CONCLUSIONS

We demonstrate fabrication of a highly efficient self-powered UV-vis photodetector based on a $ZnIn_2S_4$ nanopetal film with a surface-dispensed agarose gel. The $ZnIn_2S_4$ nanopetals films are grown on FTO-coated glass hydrothermally. The photoresponse of the $ZnIn_2S_4$/gel hybrid device is seen to be higher by a factor of ~100 even for zero bias as compared to the photodetector without gel powered at −1.5 V. The response times (rise and fall) for the $ZnIn_2S_4$ only (i.e. without gel) photodetector is 2 ms (for both), whereas the response times for the $ZnIn_2S_4$-gel hybrid device is 25 ms and 120 ms, respectively. Impedance spectroscopy shows a drastic change in the charge transfer resistance and capacitance in the hybrid device under illumination. The hybrid photodetector shows good responsivity of 16.5 mA/W even at zero bias.

## ASSOCIATED CONTENT

### Supporting Information

Rise and decay time of the FTO-$ZnIn_2S_4$-Pt device and FTO-$ZnIn_2S_4$-gel-Pt device, I−V linear plot of $ZnIn_2S_4$-gel-Pt in the dark, current vs voltage linear and semilog plot and comparison of photodetector properties of a doctor-bladed thin film with hydrothermally grown nanopetal film. This information is available free of charge via the Internet at http://pubs.acs.org/.

## AUTHOR INFORMATION

### Corresponding Author

*E-mail: sb.ogale@ncl.res.in, satishogale@gmail.com.

### Author Contributions

The manuscript was written through contributions of all authors. All authors have given approval to the final version of the manuscript. L.M. and N.S.C. contributed equally.

### Notes

The authors declare no competing financial interest.

## ACKNOWLEDGMENTS

This work is supported by the Council of Scientific and Industrial Research (CSIR, Govt. of India). The authors would like to acknowledge Dr. B. B. Kale (C-MET, Pune) for FESEM characterization facility. L.M. would like to acknowledge fellowship support by CSIR.

## ABBREVIATIONS

FTO = fluorine doped tin oxide
IPCE = incident photon conversion efficiency

## REFERENCES

(1) Yin, Z.; Li, H.; Li, H.; Jiang, L.; Shi, Y.; Sun, Y.; Lu, G.; Zhang, Q.; Chen, X.; Zhang, H. *ACS Nano* **2012**, *6*, 74−80.
(2) Hu, P. A.; Wang, L.; Yoon, M.; Zhang, J.; Feng, W.; Wang, X.; Wen, Z.; Idrobo, J. C.; Miyamoto, Y.; Geohegan, D. B.; Xiao, K. *Nano Lett.* **2013**, *13*, 1649−1654.
(3) Hu, P. A.; Wen, Z.; Wang, L.; Tan, P.; Xiao, K. *ACS Nano* **2012**, *6*, 5988−5994.
(4) Peng, S.; Zhu, P.; Thavasi, V.; Mhaisalkar, S. G.; Ramakrishna, S. *Nanoscale* **2011**, *3*, 2602−2608.
(5) Peng, S.; Zhu, P.; Mhaisalkar, S. G.; Ramakrishna, S. *J. Phys. Chem. C* **2012**, *116*, 13849−13857.
(6) Chaudhari, N. S.; Bhirud, A. P.; Sonawane, R. S.; Nikam, L. K.; Warule, S. S.; Rane, V. H.; Kale, B. B. *Green Chem.* **2011**, *13*, 2500−2506.
(7) Romeo, N.; Dallaturca, A.; Braglia, R.; Sberveglieri, G. *Appl. Phys. Lett.* **1973**, *22*, 21.
(8) Chen, Y.; Huang, R.; Chen, D.; Wang, Y.; Liu, W.; Li, X.; Li, Z. *ACS Appl. Mater. Interfaces* **2012**, *4*, 2273−2279.
(9) Chen, Y.; Hu, S.; Liu, W.; Chen, W.; Wu, L.; Wang, X.; Liua, P.; Li, Z. *Dalton Trans.* **2011**, *40*, 2607−2613.
(10) Yang, Y.; Guo, W.; Qi, J.; Zhao, J.; Zhang, Y. *Appl. Phys. Lett.* **2010**, *97*, 223113.
(11) Bie, Y.-Q.; Liao, Z.-M.; Zhang, H.-Z.; Li, G.-R.; Ye, Y.; Zhou, Y.-B.; Xu, J.; Qin, Z.-X.; Dai, L.; Yu, D.-P. *Adv. Mater.* **2011**, *23*, 649−653.
(12) Hatch, S. M.; Briscoe, J.; Dunn, S. *Adv. Mater.* **2013**, *25*, 867−871.
(13) Li, X.; Gao, C.; Duan, H.; Lu, B.; Wang, Y.; Chen, L.; Zhang, Z.; Pan, X.; Xie, E. *Small* **2013**, *9*, 2005−2011.
(14) Li, X.; Gao, C.; Duan, H.; Lu, B.; Pan, X.; Xie, E. *Nano Energy* **2012**, *1*, 640−645.
(15) Koo, H.-J.; Chang, S. T.; Velev, O. D. *Small* **2010**, *6*, 1393−1397.
(16) Cayre, O. J.; Chang, S.T.; Velev, O. D. *J. Am. Chem. Soc.* **2007**, *129*, 10801−10806.
(17) Koo, H.-J.; So, J.-H.; Dickey, M. D.; Velev, O. D. *Adv. Mater.* **2011**, *23*, 3559−3564.
(18) Koo, H.-J.; Chang, S. T.; Slocik, J. M.; Naik, R. R.; Velev, O. D. *J. Mater. Chem.* **2011**, *21*, 72−79.
(19) Han, J.-H.; Kim, K. B.; Kim, H. C.; Chung, T. D. *Angew. Chem.* **2009**, *121*, 3888−3891.
(20) Mandal, L.; Deo, M.; Yengantiwar, A.; Banpurkar, A.; Jog, J.; Ogale, S. *Adv. Mater.* **2012**, *24*, 3686−3691.
(21) Gautam, V.; Bag, M.; Narayan, K. S. *J. Phys. Chem. Lett.* **2010**, *1*, 3277−3282.
(22) Valpolin, A. A.; Nikolaev, Yu. A.; Rud, V. Yu.; Rud, Yu. V.; Terukov, E. I.; Fernelius, N. *Semiconductors* **2003**, *37*, 178-191−802.
(23) Guo, F.; Yang, B.; Yuan, Y.; Xiao, Z.; Dong, Q.; Bi, Y.; Huang, J. *Nat. Nanotechnol.* **2012**, *7*, 798.
(24) Ghosh, M.; Raychaudhuri, A. K. *Appl. Phys. Lett.* **2011**, *98*, 153109.